

Supporting Information

Controlled Assembly of Block Copolymer Coated Nanoparticles in 2D Arrays

*Vanessa B. Leffler⁺, Lina Mayr⁺, Paul Paciok, Hongchu Du, Rafal E. Dunin-Borkowski, Martin Dulle, and Stephan Förster**

[ange_201901913_sm_miscellaneous_information.pdf](#)

Table of content

Correlation functions.....	3
Extraction of particle coordinates from TEM images	3
Bond Orientational Order (BOO).....	3
3D reconstruction of the monolayer.....	6
Influence of concentration	7
Additional Information.....	8
Experimental Section.....	9
Polymer synthesis.....	9
Nanoparticle syntheses.....	9
Ligand exchange	10
TEM sample preparation.....	10
Methods	10
Polymer characterization	11
SEC measurements.....	11
NMR spectra.....	12
Literature	18

Correlation functions

Extraction of particle coordinates from TEM images

All particle positions were extracted using the software imageJ with its particle analysis tool. First the scale was set using the scale bar in the image then a band pass filter was used to flatten the background of the pictures. Subsequently, a threshold filter was used to separate the particles from the background using the original image as reference. Then the particle analysis tool was used to extract the particle coordinates. These coordinates were then used with our own software to calculate the bond orientational order (BOO), the radial distribution function $g(r)$ and coordination numbers.

Bond Orientational Order (BOO)

One way to characterize an ordered system that has multiple domains or is not perfectly ordered is to use the bond orientational order. This Parameter reflects the orientational arrangement of next neighbors within a given set of coordinates. The BOO is defined as

$$\chi_m = \left\langle \left| \frac{1}{N_B} \sum_r \exp(im\theta_r) \right|^2 \right\rangle$$

m is the rotational order, θ_r is the angle between the reference axis and a bond vector between next neighbor particles with one of them at the distance r . N_B is the number of next neighbor bonds and the angle brackets should indicate an ensemble average. In the literature most of the time the reference vector is fixed for all bond vectors and the global BOO with respect to this reference vector is obtained. What we do instead is calculate a local BOO for each particle by mapping all its next neighbor bonds and make one of them the reference vector. This has the distinct advantage that the resulting BOO values will be independent of the choice of a global reference vector. When using the same reference vector for all bonds the choice of this vector can have a great impact when comparing different sample sets and how they are oriented with respect to each other. We tested the method extensively and found that it was much more robust, in the sense that samples with the same number of domains and sizes but differing orientation between domains would give the same averaged values for the BOO than with the global method. The only parameter that heavily influences the outcome of this analysis is the choice of the cutoff distance for next neighbors. The cut-off distance is chosen so that the first peak in the $g(r)$ is completely encompassed and is given for each investigated sample. All distances are in nm.

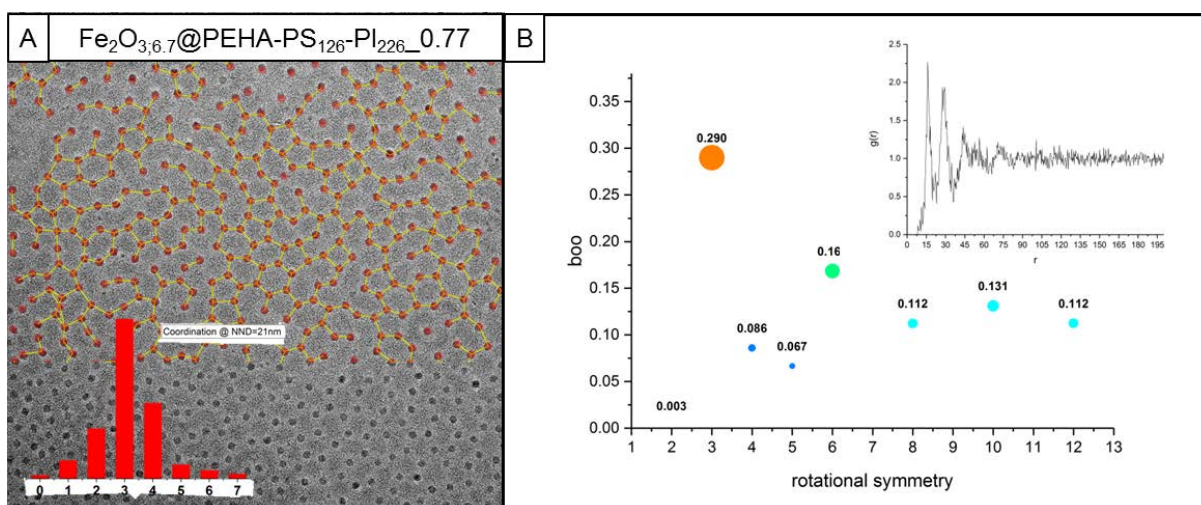


Figure S1: A: TEM image of Fe₂O_{3:3.6.7}@PEHA-PS₁₂₆-PI₂₂₆_0.77 with some of the extracted coordinates shown in red; the inset shows the coordination histogram with a distinct peak at three next neighbors. B: The associated BOO values for various rotational symmetries; the inset shows the radial distribution function.

With this method we investigated the BOO for the Fe₂O_{3:3.6.7}@PEHA-PS₁₂₆-PI₂₂₆_0.77 (Fig. S1), Fe₂O_{3:3.5.5}@PEHA-PS₁₂₆-PI₁₈₄_0.7 (Fig. S2) and Fe₂O_{3:3.5.5}@PEHA-PS₁₂₆-PI₁₈₄_0.16 (Fig. S3). All three samples were prepared with a different grafting density resulting in different structures.

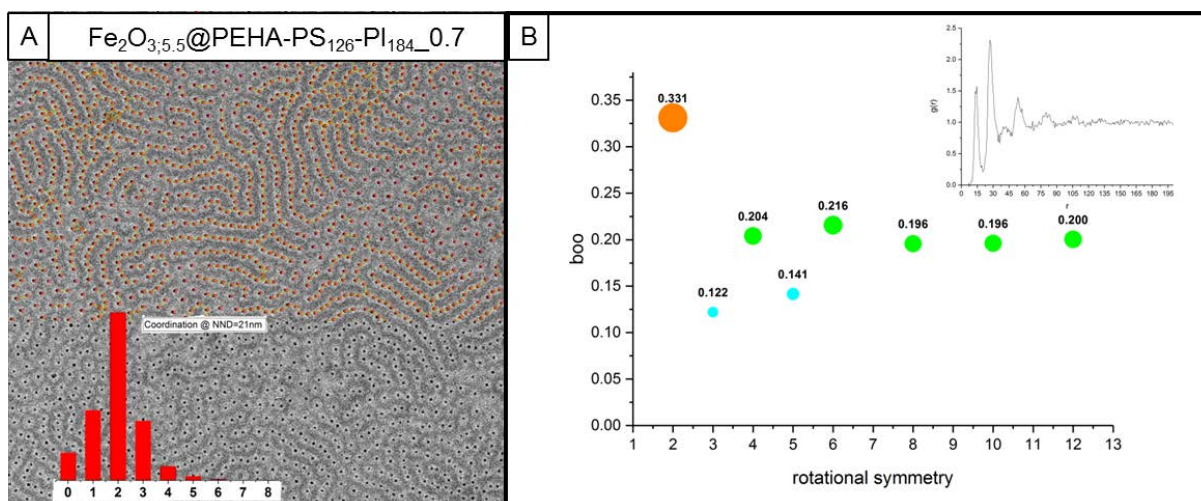


Figure S2: A: TEM image of $\text{Fe}_2\text{O}_{3,5.5}@PEHA-PS_{126}-PI_{184}_0.7$ with some of the extracted coordinates shown in red; the inset shows the coordination histogram with a distinct peak at two next neighbors. B: The associated BOO values for various rotational symmetries; the inset shows the radial distribution function.

The samples $\text{Fe}_2\text{O}_{3,6.7}@PEHA-PS_{126}-PI_{226}_0.77$ and $\text{Fe}_2\text{O}_{3,5.5}@PEHA-PS_{126}-PI_{184}_0.7$ have a significantly increased BOO value for 3 and 2-fold rotational symmetry, respectively. This is further proof that the structures we claimed are indeed forming. These samples furthermore show nicely the high degree of control over the particle position we have as not only are the particles well and evenly separated but also show a preference for the number of next neighbors. Due to the formation of a network like structure no BOO value is significantly larger than for a randomly distributed set of particles for $\text{Fe}_2\text{O}_{3,5.5}@PEHA-PS_{126}-PI_{184}_0.16$.

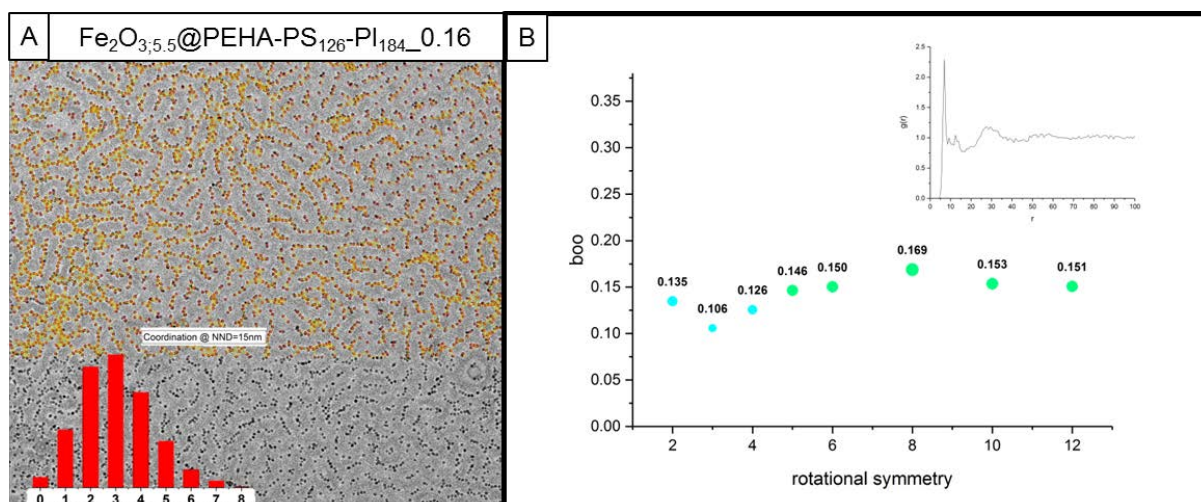


Figure S3: A: TEM image of $\text{Fe}_2\text{O}_{3,5.5}@PEHA-PS_{126}-PI_{184}_0.16$ with some of the extracted coordinates shown in red; the inset shows the coordination histogram with no preferred coordination number. B: The associated BOO values for various rotational symmetries; the inset shows the radial distribution function.

The results from our picture analysis allow us to quantitatively compare our samples to the literature ^[1] see Fig. S4. In this way we were able to show that the order obtained in our system is more defined due to the method we developed.

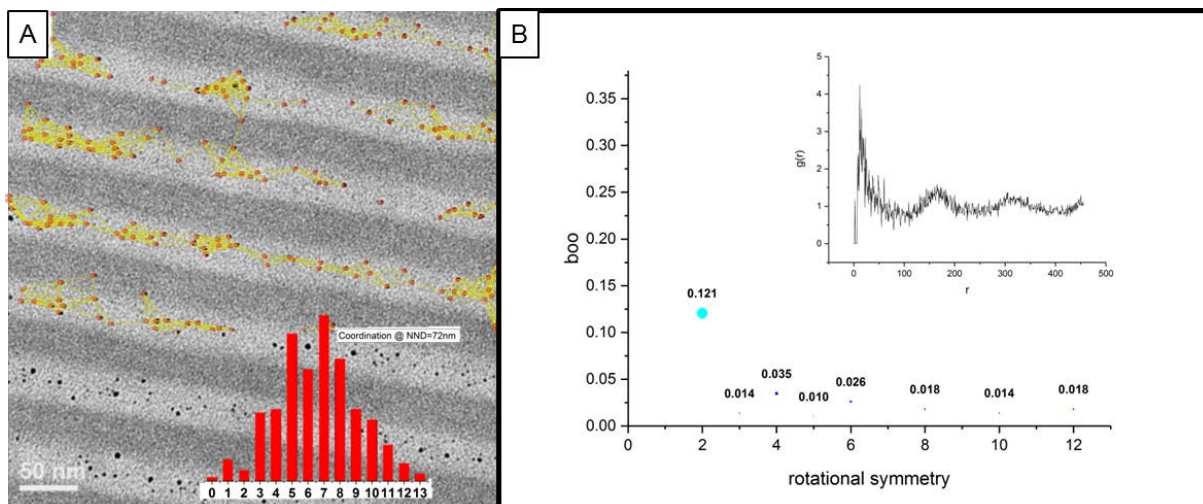


Figure S4: A: TEM image taken from Kim *et al.*^[1] with some of the extracted coordinates shown in red; the inset shows the coordination histogram with no preferred coordination number. B: The associated BOO values for various rotational symmetries; the inset shows the radial distribution function.

3D reconstruction of the monolayer

The monolayers were prepared on carbon-coated TEM copper grids. For EM tomography, monolayers that had been prepared from block-copolymer-coated nanoparticles in $\text{Fe}_2\text{O}_{3,6.7}@\text{PEHA-PS}_{126}\text{-PI}_{226}_{0.77}$ were studied using STEM tomography. Figure S5 shows a three-dimensional reconstruction of the nanoparticles.

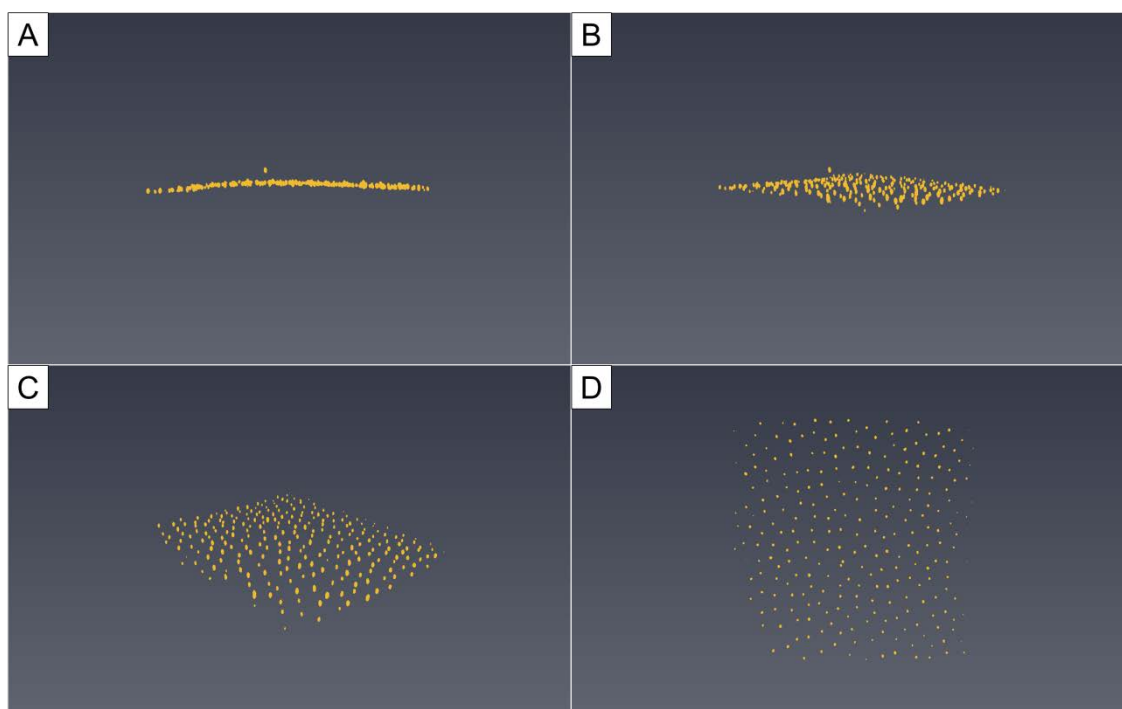


Figure S5: Three-dimensional reconstruction of nanoparticles in $\text{Fe}_2\text{O}_{3,6.7}@\text{PEHA-PS}_{126}\text{-PI}_{226}_{0.77}$ recorded using STEM tomography. The nanoparticles are viewed (A) from the side, (B) slightly tilted, (C) tilted and (D) from the top view.

The three-dimensional reconstruction shows that the block copolymer coated nanoparticles form a monolayer. This observation is supported by the fact that a single nanoparticle is visible on top of the monolayer in Figs 3A and 3B. The fact that this nanoparticle can be clearly distinguished from the nanoparticles that are incorporated into the monolayer confirms that monolayers and double layers can be distinguished from each other.

Influence of concentration

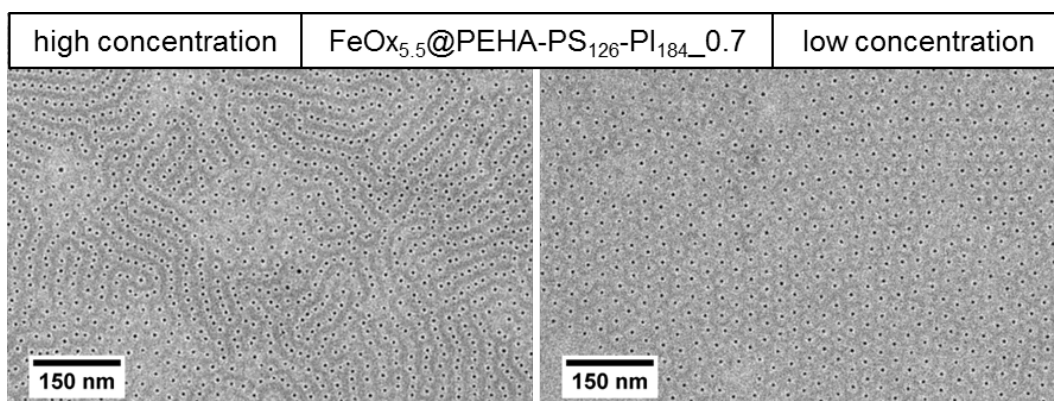


Figure S6: TEM images of the different structures obtained from the same coated nanoparticles at different concentration in solution.

All self-assembled structures were formed from a sufficiently large concentration (0.6 – 1.2 mg/mL) of the solution to achieve the formation of homogeneous, large and continuous monolayers. Fig. S6 shows the effect of using a significantly lower concentration of the solution during self-assembly. Instead of the ordered stripe domains containing ordered nanoparticle arrays, we observe the formation of hexagonally arranged spherical nanoparticle/PS-domains. This indicates that repulsive steric interactions for the solvent-swollen nanoparticle-block copolymer conjugates lead to local spherical arrangements. The steric repulsion is screened for higher concentrations around the overlap concentration which is the concentration range, where the experiments were routinely performed. Additionally, the low concentration of the solution makes an interaction of the coated nanoparticles significantly less likely. Thus, the polymer cannot act as template for the assembly.

Additional Information

In order to show the wide applicability of this method we additionally prepared samples with ZnO and Cu₂ZnSnS₄ (CZTS) nanoparticles, respectively. The ZnO nanoparticles are very small with an average diameter of 3.7 nm, while the Cu₂ZnSnS₄ nanoparticles are comparable large with an average diameter of 13.7 nm. Furthermore, the Cu₂ZnSnS₄ nanoparticles have a distribution of 18%. The nanoparticles were coated with a PI-PS-PEHA block copolymer of about 28000 g/mol aiming for a medium grafting density. In both cases the expected strip-like structures can be observed. This demonstrates that the proposed method works with a wide variety of nanoparticles but also with a variety of sizes and less monodisperse nanoparticles.

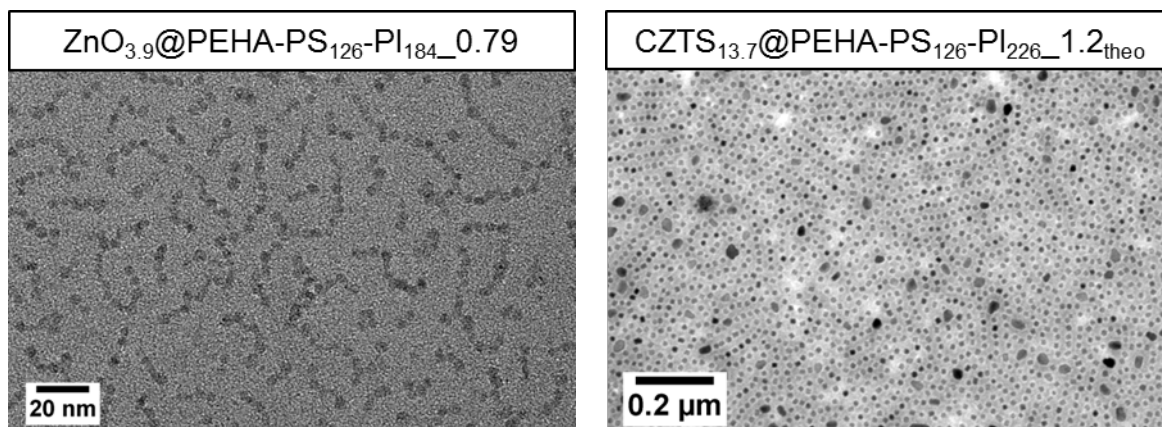


Figure S7: TEM images of block copolymer coated ZnO nanoparticles (left) and Cu₂ZnSnS₄ nanoparticles (right). The CZTS nanoparticles have a rather high polydispersity which makes determination of the grafting density pointless.

Table S1. Theoretical end-to-end distances (R_{theo}), half strip thickness for the neat block copolymers (R_{meas}) and half strip thickness for the strip-like structure with the nanoparticles (R_{struc}) for the perspective blocks of the block copolymers. (¹ the nanocomposites contain PbS nanoparticles, ² the nanocomposites contain Fe₂O₃ nanoparticles)

Molecular weight	R_{theo} [nm]		R_{meas} [nm]		R_{struc} [nm]	
	PS	PI	PS	PI	PS	PI
16300 g/mol ¹	6.1	6.9	could not be measured			
25650 g/mol ²	7.7	8.6	No data		5.0±0.6	4.6±0.8
28500 g/mol ¹	7.7	9.5	6.5±0.8	5.4±0.9	4.5±0.9	5.4±0.9
48500 g/mol ¹	10.3	12.1	9.1±1.0	9.0±1.2	8.8±1.2	8.0±1.5

R_{theo} was calculated as follows:

$$R_{theo} = b_i \cdot \sqrt{N_{K,i}} = b_i \cdot \sqrt{\frac{M_i}{M_{0,i}}}$$

Here b_i is the Kuhn length ($b_{PS} = 1.8$ nm; $b_{PI} = 0.84$ nm), $N_{K,i}$ is the number of Kuhn segments and $M_{0,i}$ is the molar mass of one Kuhn segment ($M_{0,PS} = 720$ g/mol; $M_{0,PI} = 120$ g/mol).

Experimental Section

Polymer synthesis

Anionic polymerization of PI₁₁₇-PS₈₀-OH, PI₂₂₆-PS₁₂₆-OH, PI₃₆₈-PS₂₂₅-OH

Cyclohexane (Aldrich) and tetrahydrofuran (THF, Aldrich) were dried with a sodium/potassium alloy and benzophenone (ACROS Organics, 99%, pure) for several days. Isoprene (Aldrich, 99%, <1000 ppm *p-tert*-butylcatechol) and styrene (Aldrich, Reagent Plus, ≥99%, contains 4-*tert*-butylcatechol as stabilizer) were dried over calcium hydride (Aldrich, powder, 0-2nm, reagent grade, ≥90%) and di-*n*-butylmagnesium (Aldrich, 1.0 M in heptane). Ethylene oxide (Air Liquide) was dried over calcium hydride and *n*-butyllithium (Aldrich, 2.5 M in hexane).

Isoprene was added to the solvent cyclohexane and the polymerization was started by injecting *sec*-BuLi (Aldrich, 1.4 M in cyclohexane). The solution was stirred at 30 °C over night. The styrene was added and the solution was stirred over night at 40 °C. THF was added as an additional solvent, before the ethylene oxide was added. The polymerization was terminated by the addition of acetic acid. Subsequently, the polymer was purified and dried.

Anionic polymerization of PI₁₈₄-PS₁₂₆-OH

Benzene (Merck, 99.5%) was dried over *n*-BuLi and styrene. Isoprene was degassed and dried once over di-*n*-butylmagnesium and once over *n*-BuLi. Styrene was degassed and dried two times over di-*n*-butylmagnesium. Ethylene oxide was degassed and dried two times over calcium hydride.

First benzene and then isoprene were added to *t*-BuLi (Aldrich, 1.7 M in pentane) and the polymerization was started by defrosting the flask. The solution was stirred over night. The styrene was added and the solution was stirred over night. The ethylene oxide was added and the solution was stirred for several hours before the polymerization was terminated by the addition of acetic acid. Subsequently, the polymer was purified and dried.

Functionalization with PEHA

The hydroxyl end functionalized polymer was dissolved in chloroform (Aldrich, anhydrous, contains amylenes as stabilizer, ≥99%) and the solution was then added to a solution of carbonyldiimidazol (CDI, Aldrich, reagent grade, 25-fold excess) in chloroform. The solution was stirred over night, before it was extracted three times with water and dried under vacuum. Pentaethylene hexamine (PEHA, Aldrich, technical grade, 25-fold excess) was dissolved in chloroform and the solution of the activated polymer in chloroform was added dropwise. The solution was stirred over night, before it was extracted three times with water and subsequently dried under vacuum.

Nanoparticle syntheses

PbS nanoparticle

In a typical synthesis lead (II) oleate was synthesized in-situ by dissolving 1.5 mmol of lead (II) acetate trihydrate (Aldrich, ACS reagent, ≥99%) and 3 mmol of oleic acid (Alfa Aesar, Tech. 90%) in 60 mL of 1-octadecene (Aldrich, technical grade, 90%). The mixture was purged for 1 hour at 110 °C. Subsequently, the solution was heated up to 140 °C before 0.75 mmol of bis(trimethylsilyl) sulfide (0.5 mol/L in octadecene, Aldrich, synthesis grade) were injected. The resulting solution was cooled to 90 °C and held there for 3 hours. The purification was done by precipitation with acetone and subsequent centrifugation. The obtained nanoparticles were redispersed in THF.

ZnO nanoparticles

The synthesis was done according to Ehlert *et al.*^[2] Zinc oleate was used as a precursor for the synthesis. It was prepared from zinc chloride (Aldrich, puriss p.a., ACS reagent, ≥98%) and sodium oleate (TCI, >97%). 0.25 mol of zinc chloride were dissolved in 500 mL of water and then added to a solution of 0.5 mol of sodium oleate in water. The white precipitate was purified by filtering and subsequent washing with water. Afterwards, the zinc oleate was dried.

In a typical nanoparticle synthesis 16 mmol of zinc oleate were dissolved in 300 mL of THF. The solution was heated to 60 °C and a solution of 16 mmol of potassium hydroxide (Aldrich, ACS reagent, ≥85%) in 16 mL of methanol (Aldrich, puriss p.a. ACS reagent, ≥99.8%) was added. The reaction mixture was held at 60 °C for several hours. After cooling to room temperature an excess of ethanol (VWR, 96%) was added and the white precipitate was purified by centrifugation. Subsequently, it was redispersed in THF.

FeOx nanoparticles

The synthesis was based on a synthesis instruction by Hyeon *et al.*^[3] The iron oxide nanoparticles were prepared from iron(III) oleate in a thermal decomposition. The oleate was synthesized by dissolving iron(III) chloride hexahydrate (Aldrich, puriss p.a. ACS reagent, ≥99.8%) and sodium oleate in a mixture of ethanol, water and heptane (Aldrich, reagent grade, 99%). The solution was heated to 70 °C for several hours, before it was extracted three times with water and subsequently dried. For the nanoparticles the iron oleate was dissolved in 100 g of 1-octadecene and 10.3 mmol of oleic acid was added before the mixture was heated to 317 °C with 3.3 K/min. The temperature was held 317 °C for 9 min. The nanoparticles were then precipitated and purified, before they were redispersed in toluene (Aldrich, puriss p.a., ACS reagent, ≥99.7%) or THF.

According to Hyeon *et al.*^[3] the composition of the iron oxide nanoparticles is $(\gamma\text{-Fe}_2\text{O}_3)_{1-x}(\text{Fe}_3\text{O}_4)_x$ and the value of x depends on the size of the nanoparticles. The estimation is that for small nanoparticles (about 5nm) the $\gamma\text{-Fe}_2\text{O}_3$ phase is

dominating. For reason of simplification – and as we have not tested the magnetism of our synthesized nanoparticles – we will refer to all iron oxide nanoparticles as Fe₂O₃.

Cu₂ZnSnS₄ nanoparticles

The synthesis of the Cu₂ZnSnS₄ (CZTS) nanoparticles was done in a heat-up synthesis according to Shavel *et al.*^[4] 2.7 mmol of copper(II) chloride dihydrate (Aldrich, ≥99.0%), 2.4 mmol of zinc oxide (Aldrich, ≥99%) and 0.9 mmol of tin(IV) chloride pentahydrate (Aldrich, 98%) were dissolved in tetrahydrofuran. Then, 12 mmol of oleylamine (Aldrich, technical grade, 70%) and 12.6 mL of 1-octadecene were added and the mixture was purged for one hour at 175 °C. The reaction mixture was then cooled to 100 °C and a mixture of 25 mmol of tert-dodecanethiol (Aldrich, mixture of isomers, 98.5%) and 2.5 mmol of 1-dodecanethiol (Aldrich, ≥98.0%) was injected. With a heating rate of 15 K/min the reaction mixture was heated up to 250 °C, kept at 250 °C for one hour and afterwards cooled to room temperature. The nanoparticles were precipitated with a toluene/ethanol mixture (1:4) overnight. The purification was done by centrifugation and subsequently the nanoparticles were redispersed in THF.

Ligand exchange

The ligand exchange was done according to Ehlert *et al.*^[5] In order to control the grafting density, we calculated the amount of polymer which was to be added with the following equation:

$$\sigma = \frac{4 \cdot r_{NP}^3 \cdot \rho_{NP} \cdot N_A \cdot (100 - X_{NP})}{3 \cdot d_{NP}^2 \cdot M \cdot X_{NP}}$$

σ is the grafting density of the polymer on the nanoparticles surface, r_{NP} is the radius of the nanoparticles, ρ_{NP} is the density of the nanoparticles, N_A is the Avogadro constant, X_{NP} is the weight percentage of the nanoparticles, d_{NP} is the diameter of the nanoparticles and M is the molecular weight of the polymer.

TEM sample preparation

The TEM samples were prepared from a toluene or cyclohexane solution on a standard TEM grid (cooper grid coated with a thin carbon film, 400 mesh) without further treatment of the TEM grid. The concentration of the solutions was 0.6 mg/mL. The TEM grid was immersed in 8 μ L of solution and the sample was allowed to dry. The sample was then stained for about 90 min with OsO₄ vapour (4 % in water).

Methods

TEM imaging

TEM measurements were conducted with a *Zeiss CEM902* (80kV), a *Zeiss/Leo EM922 Omega* (200kV) and a *Philips CM20* (200kV).

ADF STEM imaging

Annular dark-field (ADF) scanning transmission electron microscopy (STEM) images were recorded as a function of specimen tilt angle in an FEI Titan G2 80-200 ChemiSTEM electron microscope operated at 200 kV. This microscope is equipped with a Schottky-type high brightness electron gun (X-FEG) and a probe spherical aberration corrector (CEOS DCOR). Specimen tilt angles of between -60° and +60° were used, with a tilt increment of 5° between -50° and +50° and 2.5° otherwise. The entire tilt series were recorded automatically using FEI Tomography software version 4.0, with the dynamic focus function calibrated and enabled. Each ADF STEM image had a size of 2048 \times 2048 pixels with a pixel size of 0.19 nm. The electron beam convergence semi-angle was 24 mrad and the inner collection semi-angle of the ADF detector was 43 mrad.

STEM tomography reconstruction

The images in the ADF STEM tilt series were aligned using cross correlation and binned by a factor of 2. Tomographic reconstruction was carried out using the simultaneous iterative reconstruction technique with 100 iterations. Image alignment and reconstruction were performed using FEI Inspect3D software version 4.1.2. Visualization of the final three-dimensional reconstruction was carried out using FEI Avizo software version 9.0.

Polymer characterization

SEC measurements

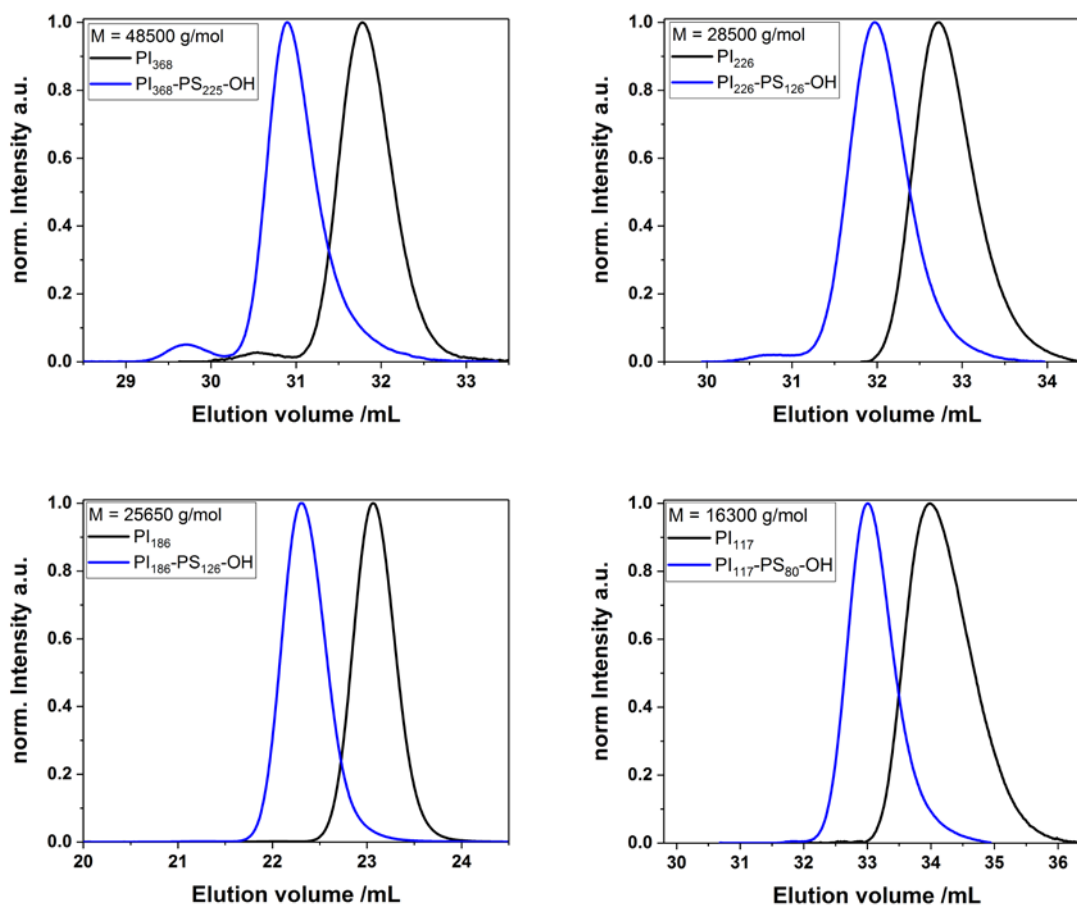


Figure 8: SEC plots for the polymers PI_{368} - PS_{225} -OH, PI_{226} - PS_{126} -OH, PI_{186} - PS_{126} -OH and PI_{117} - PS_{80} -OH. The SEC of PI_{186} - PS_{126} -OH was measured on a different setup which results in a different elution volume compared with the other measurements.

Table 2. Summary of the synthesized PI_m - PS_n -OH block copolymers. (^a determined from SEC, ^b determined from ¹H-NMR.)

	PI ^a			PS ^b			PI-PS-OH		
	M_n [g/mol]	m	f_{PI}	M_n [g/mol]	n	f_{PS}	M_n [g/mol]	PDI ^a	χ_N
PI_{117} - PS_{80} -OH	8000	117	0.53	8300	80	0.47	16300	1.04	30.3
PI_{184} - PS_{126} -OH	12550	184	0.45	13100	126	0.55	25650	1.01	47.7
PI_{226} - PS_{126} -OH	15400	226	0.58	13100	126	0.42	28500	1.03	54.1
PI_{368} - PS_{225} -OH	25100	368	0.56	23400	225	0.44	48500	1.05	91.2

NMR spectra

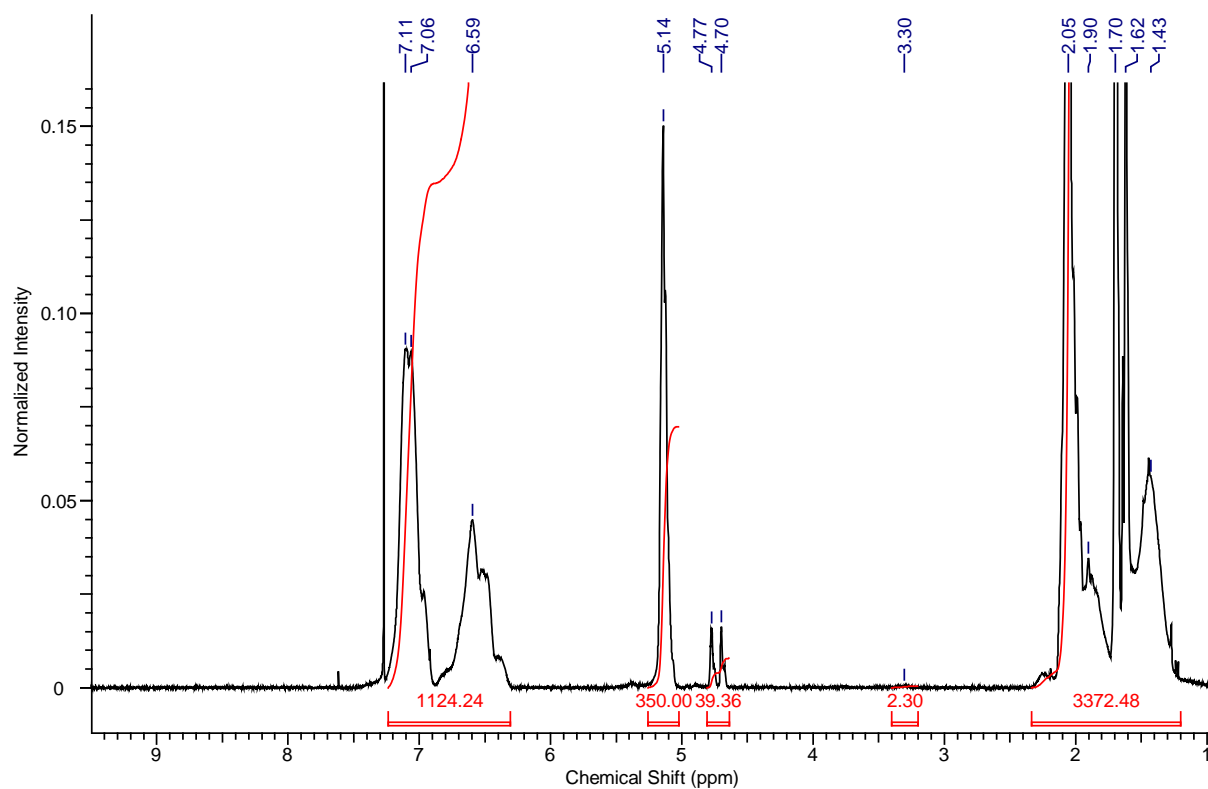


Figure 9: NMR spectrum of PI₃₆₈-PS₂₂₅-OH.

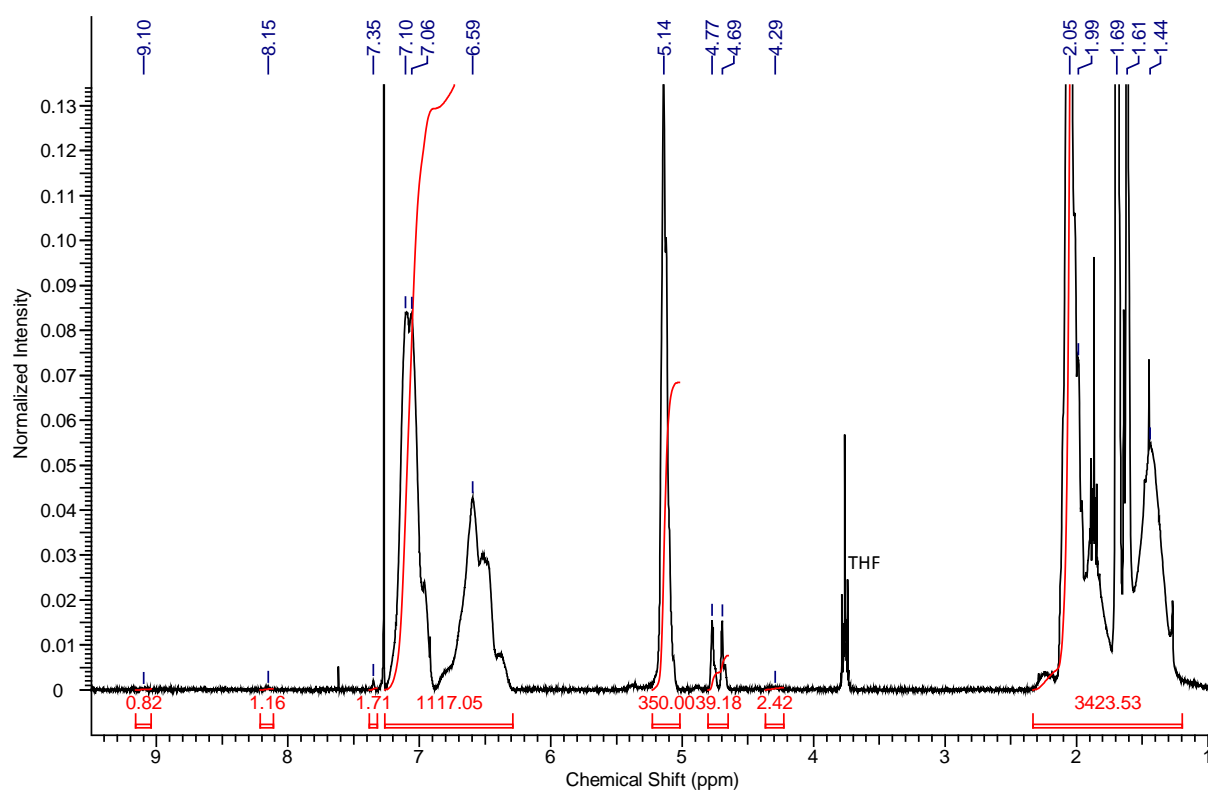


Figure 10: NMR spectrum of PI₃₆₈-PS₂₂₅-CDI.

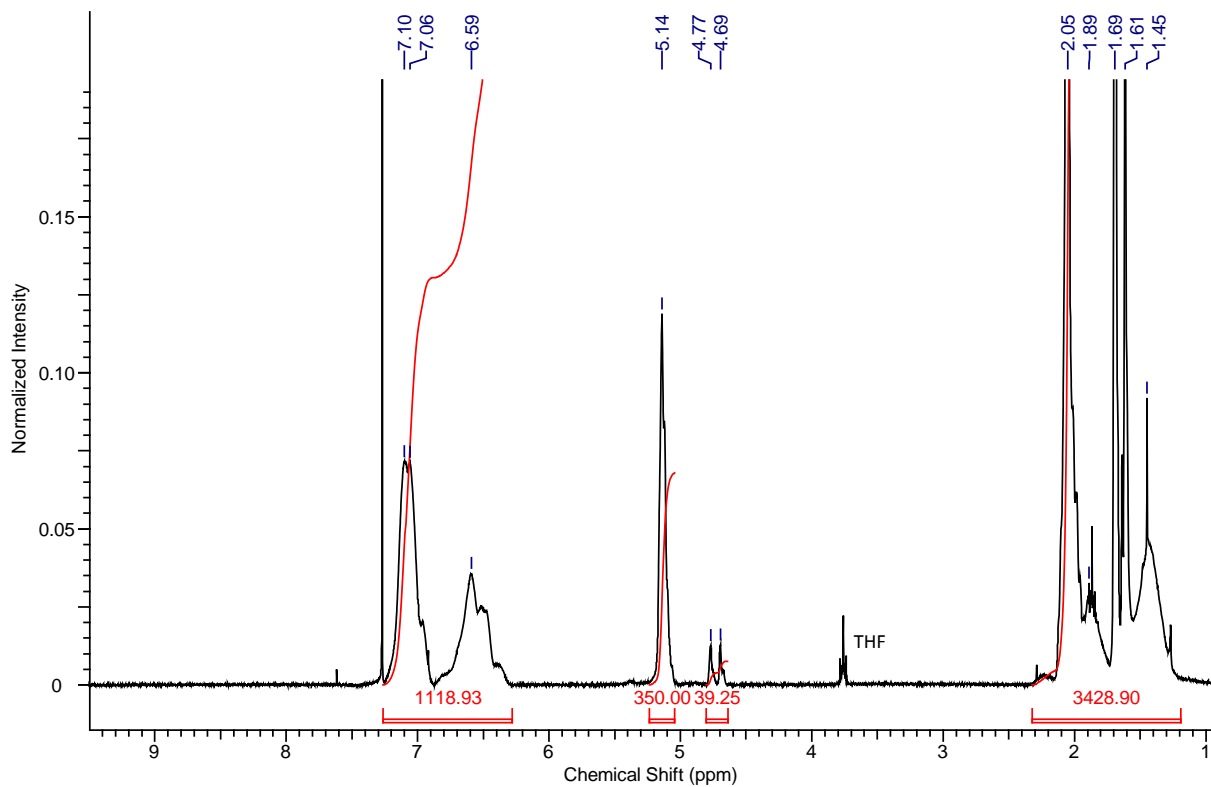


Figure 11: NMR spectrum of PI₃₆₈-PS₂₂₅-PEHA.

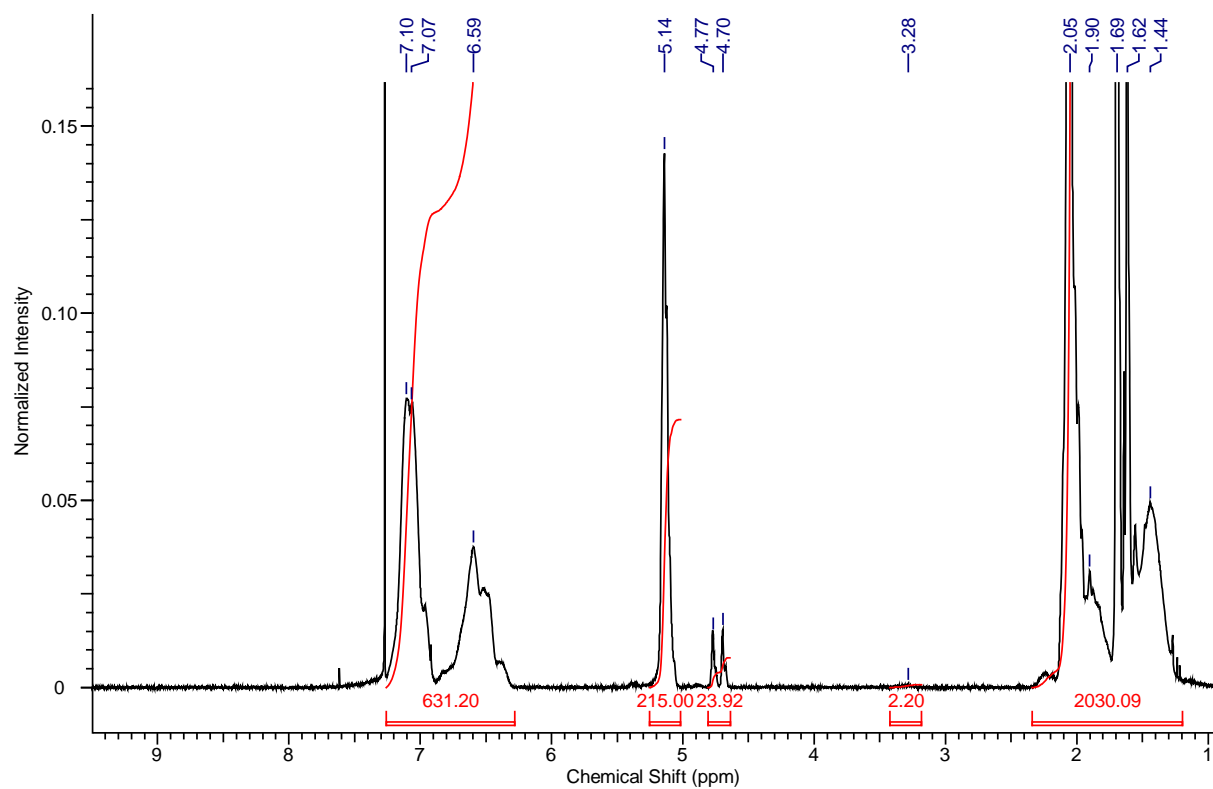


Figure 12: NMR spectrum of PI₂₂₆-PS₁₂₆-OH.

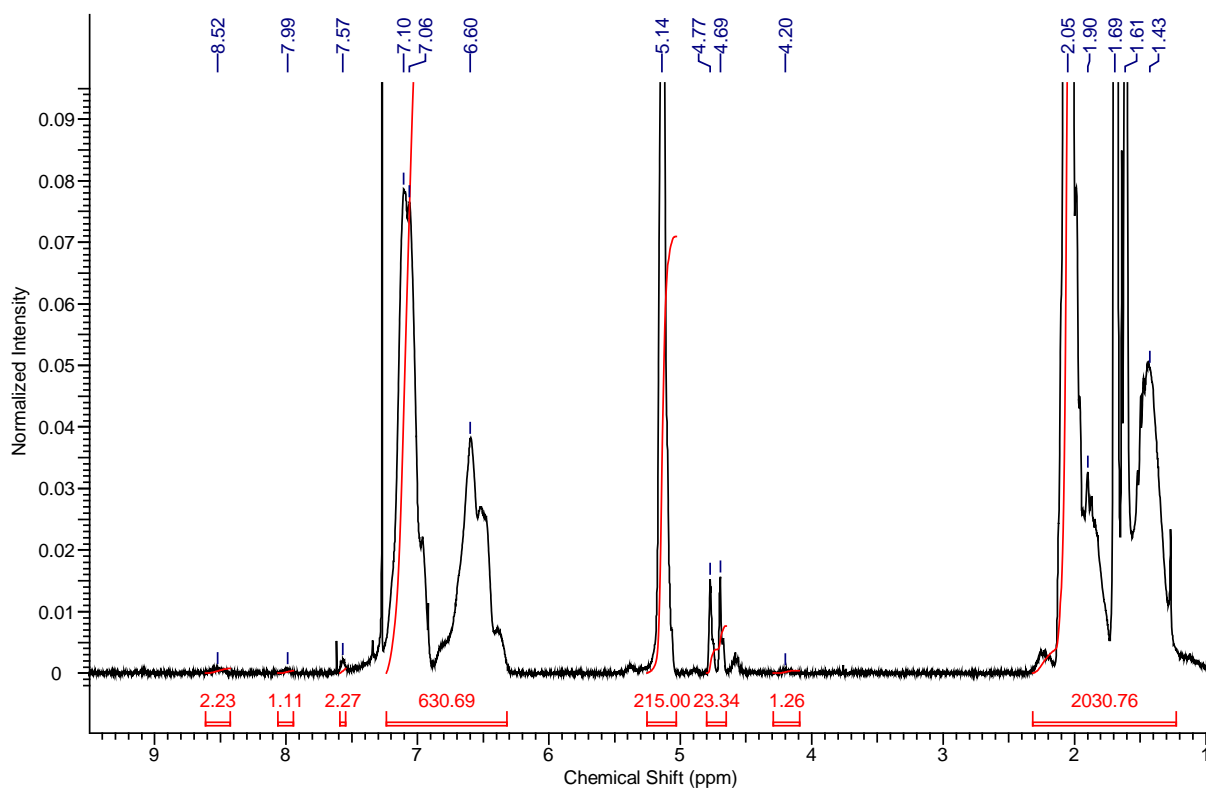


Figure 13: NMR spectrum of PI₂₂₆-PS₁₂₆-CDI.

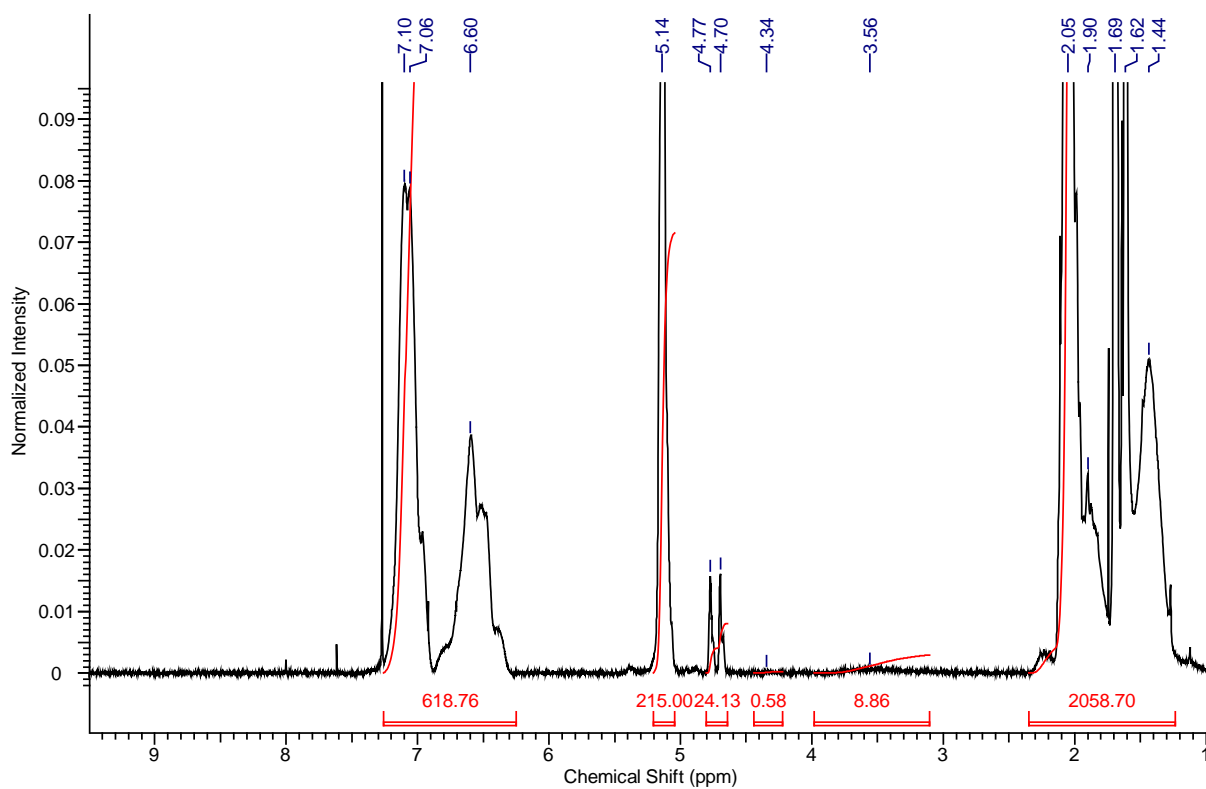


Figure 14: NMR spectrum of PI₂₂₆-PS₁₂₆-PEHA.

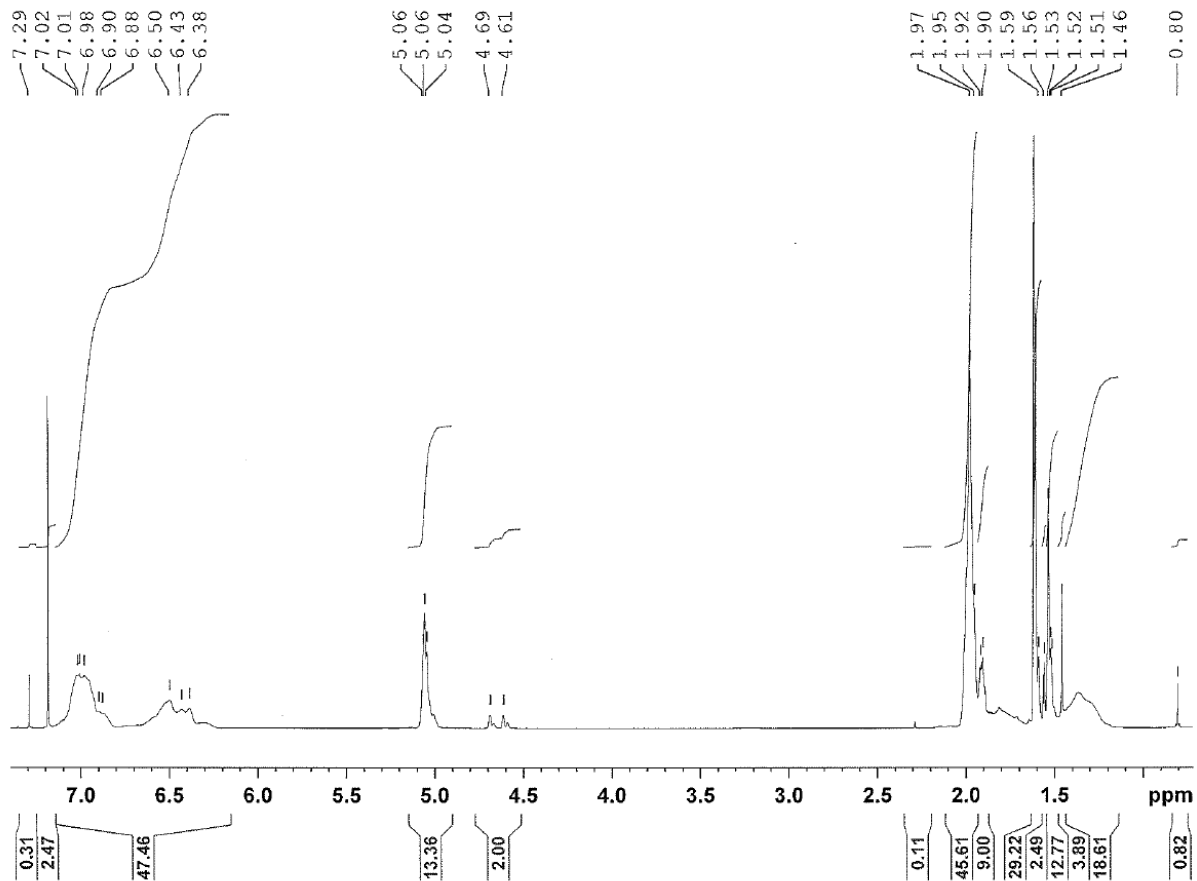


Figure 15: NMR spectrum of PI₁₈₆-PS₁₂₆-OH.

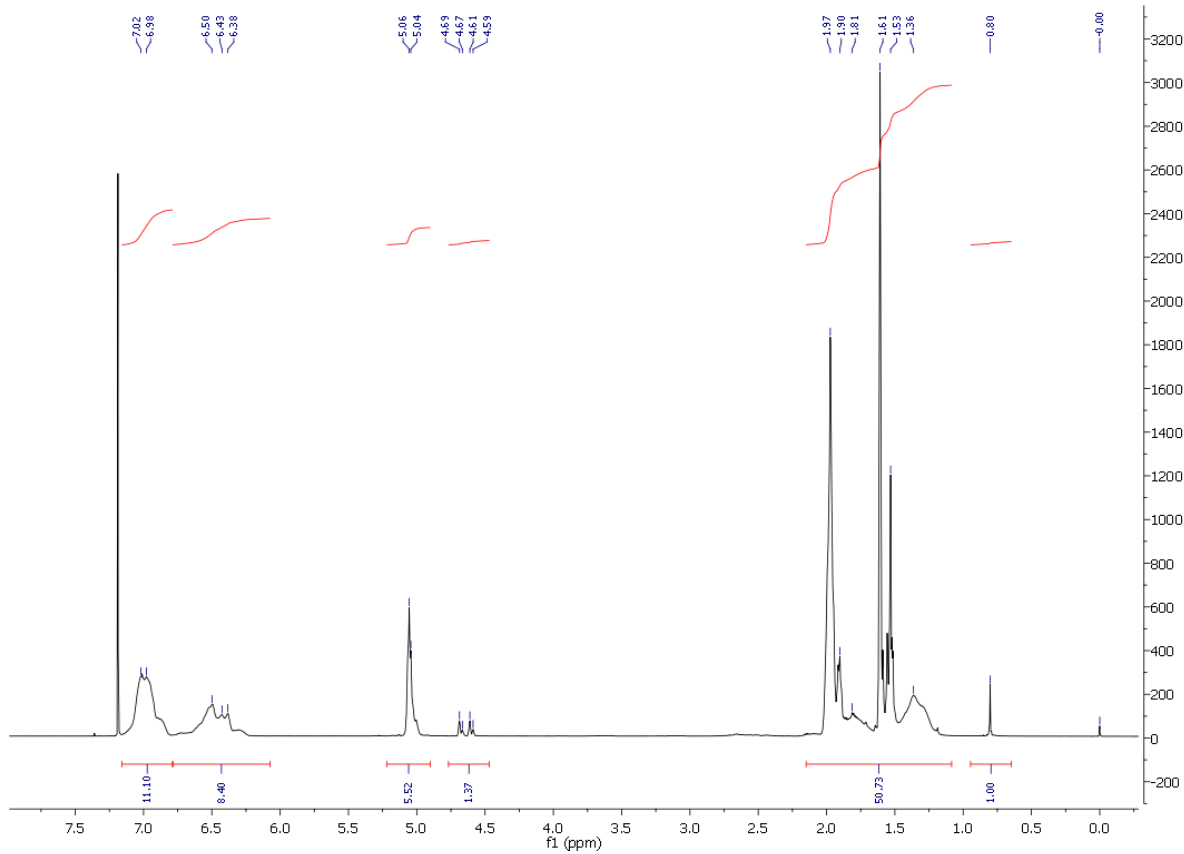


Figure 16: NMR spectrum of PI₁₈₆-PS₁₂₆-CDI.

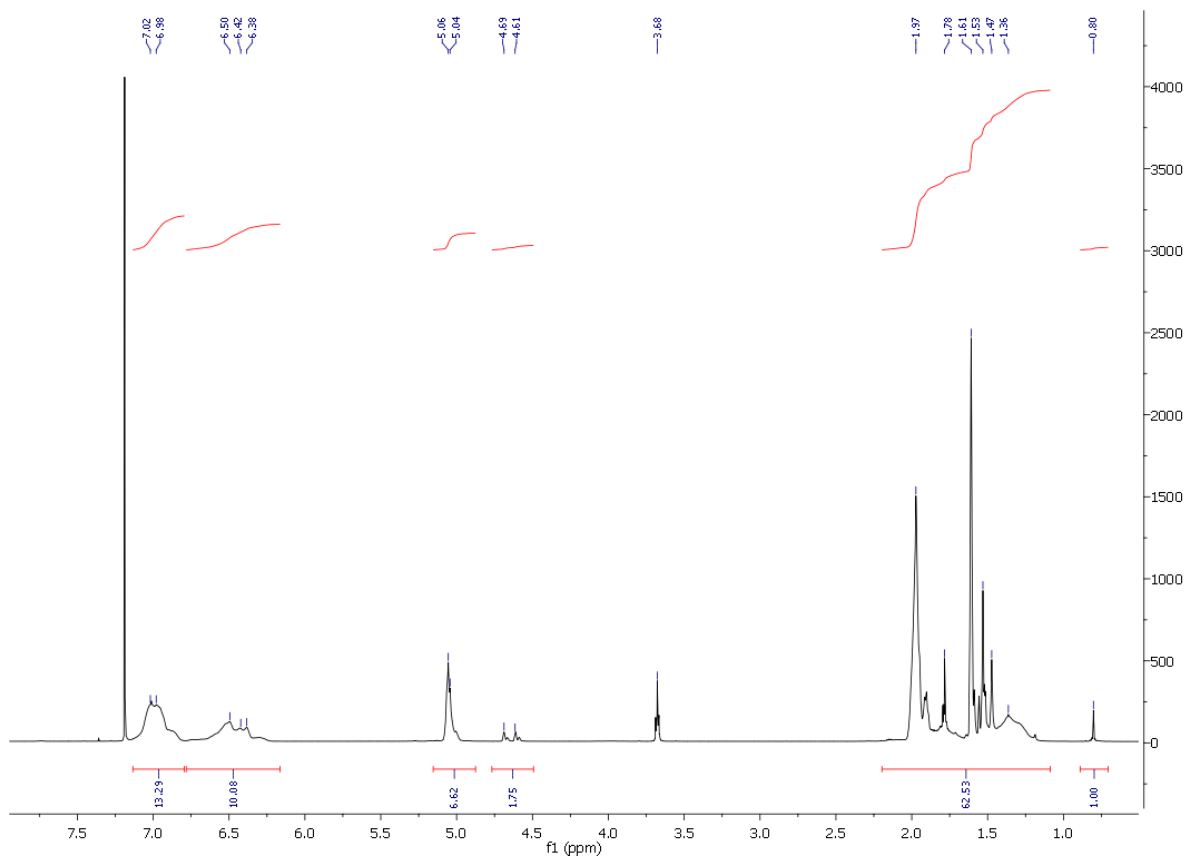


Figure 17: NMR spectrum of PI₁₈₆-PS₁₂₆-PEHA.

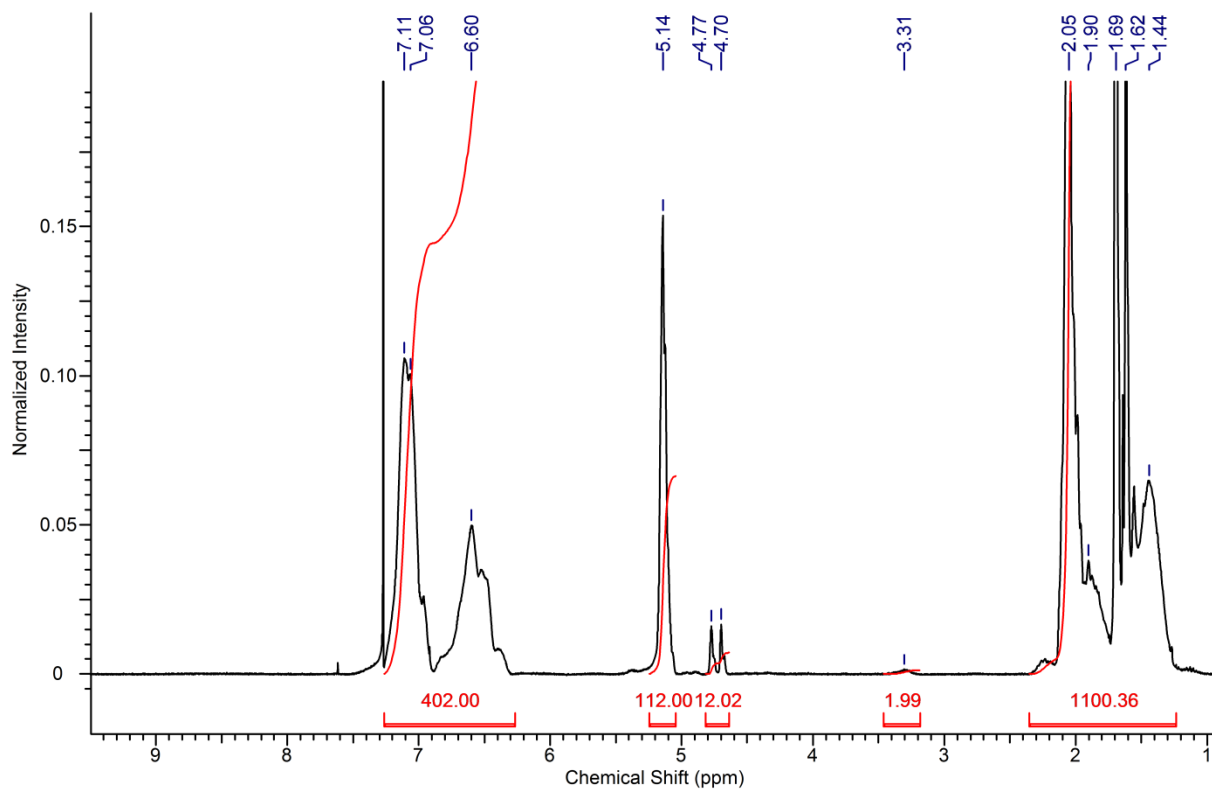


Figure 18: NMR spectrum of PI₁₁₇-PS₈₀-OH.

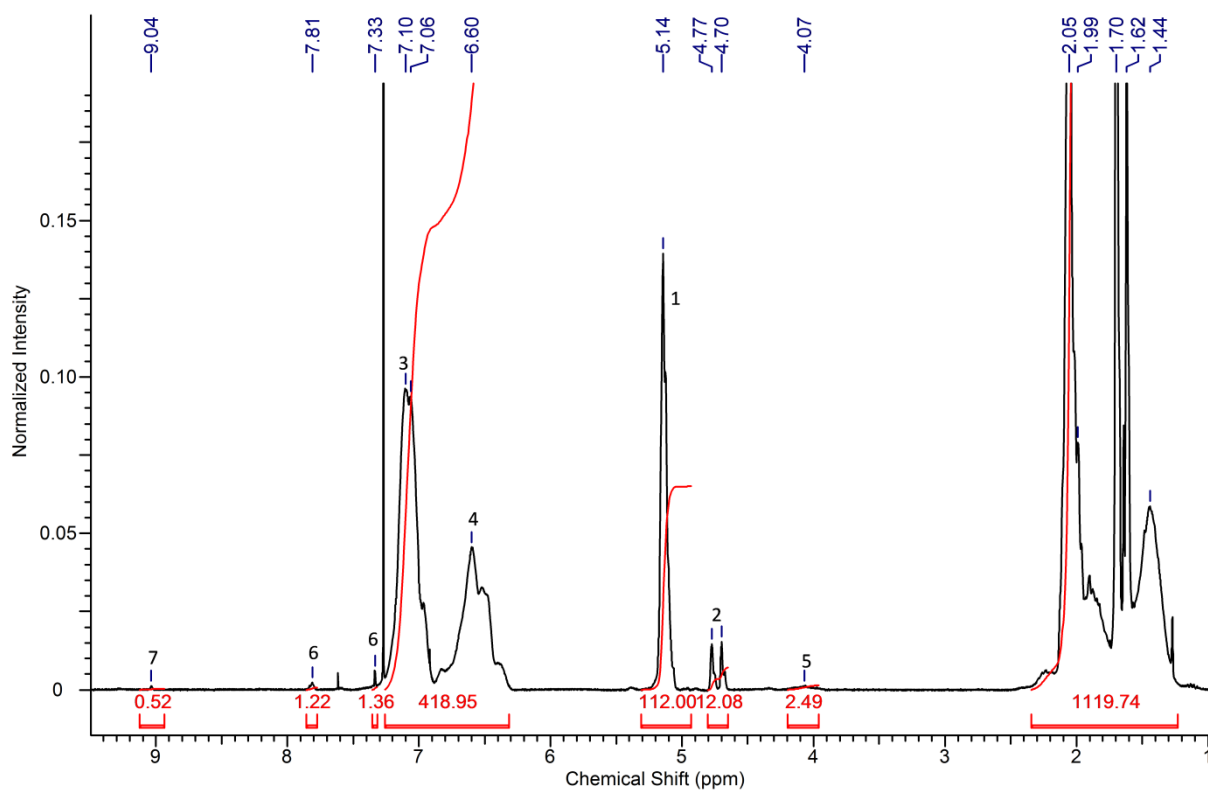


Figure 19: NMR spectrum of PI₁₁₇-PS₈₀-CDI.

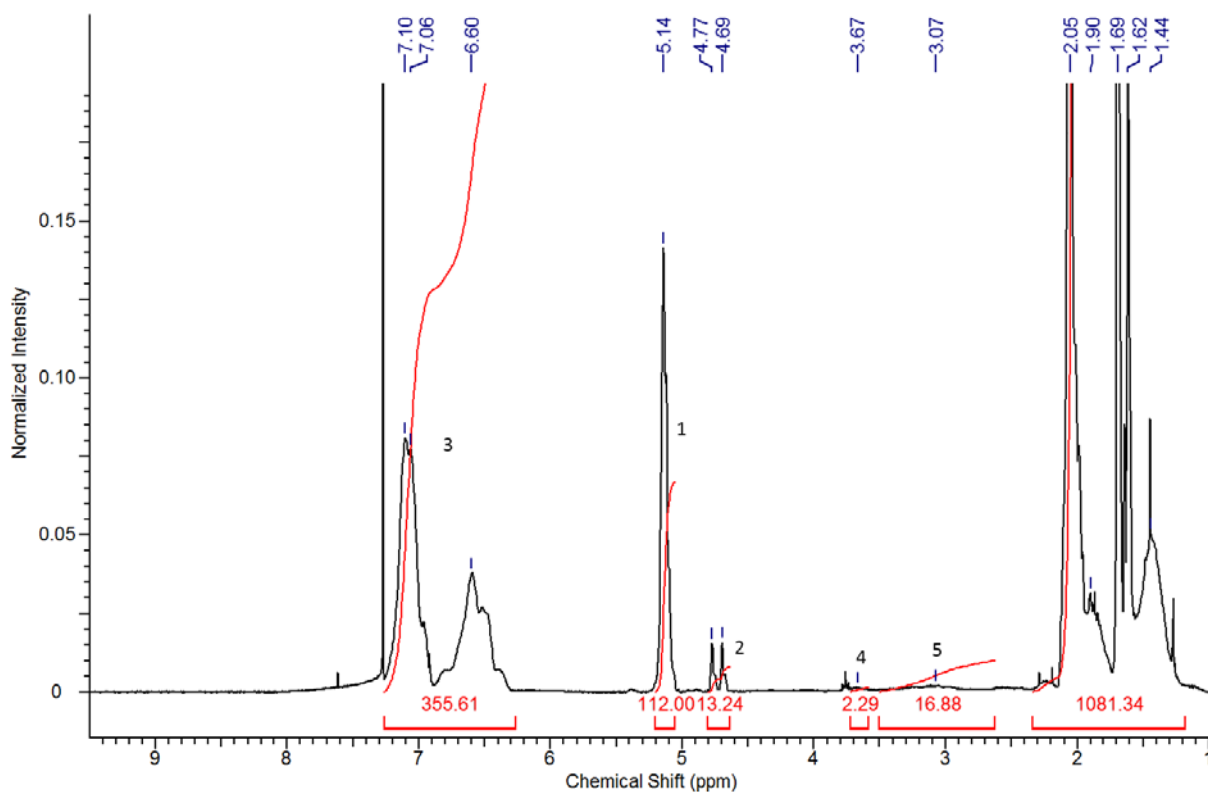


Figure 20: NMR spectrum of PI₁₁₇-PS₈₀-PEHA.

Literature

- [1] B. J. Kim, J. Bang, C. J. Hawker, J. J. Chiu, D. J. Pine, S. G. Jang, S.-M. Yang, E. J. Kramer, *Langmuir* **2007**, *23*, 12693-12703.
- [2] S. Ehlert, T. Lunkenbein, J. Brey, S. Förster, *Colloids and Surfaces A* **2014**, *444*, 76-80.
- [3] J. Park, K. An, Y. Hwang, J.-G. Park, H.-J. Noh, J.-Y. Kim, J.-H. Park, N.-M. Hwang, T. Hyeon, *Nat. Mater.* **2004**, *3*, 891-895.
- [4] A. Shavel, M. Ibáñez, Z. Luo, J. De Roo, A. Carrete, M. Dimitrievska, A. Genc, M. Meyns, A. Pérez-Rodríguez, M. V. Kovalenko, J. Arbiol, A. Cabot, *Chem. Mater.* **2016**, *3*, 720-726.
- [5] S. Ehlert, S. Mehdizadeh Taheri, D. Pirner, M. Drechsler, H.-W. Schmidt, S. Förster, *ACS Nano* **2014**, *8*, 6114-6122.